Antibacterial activity of a glass ionomer cement doped with copper nanoparticles

David AGUILAR-PEREZ[1], Rossana VARGAS-CORONADO[1], Jose M. CERVANTES-UC[1],
Nayeli RODRIGUEZ-FUENTES[1], Conrado APARICIO[2], Cristian COVARRUBIAS[3], Marco ALVAREZ-PEREZ[4],
Victor GARCIA-PEREZ[5], Miryam MARTINEZ-HERNANDEZ[5] and Juan Valerio CAUICH-RODRIGUEZ[1]

[1] Scientific Research Center of Yucatan (CICY), St 43 130, Chuburna Hidalgo, Merida, Yucatan, 97205, Mexico
[2] Minnesota Dental Research Center for Biomaterials and Biomechanics, University of Minnesota School of Dentistry, Moos Tower, 515, Delaware St SE, Minneapolis, MN 55455, USA
[3] Laboratory of Nanobiomaterials, Institute for Research in Dental Sciences, Faculty of Dentistry, University of Chile, Sergio Livingstone 943, Independencia, Santiago, Chile
[4] Tissue Bioengineering Laboratory, Division of Graduate Studies and Research of the Faculty of Dentistry, UNAM, Mexico City 04510, Mexico
[5] Laboratory of Molecular Genetics, Division of Graduate Studies and Research of the Faculty of Dentistry, UNAM, Mexico City 04510, Mexico
Corresponding author, Juan Valerio CAUICH RODRIGUEZ; E-mail: jvcr@cicy.mx

Copper nanoparticles (NCu) were synthetized and added to commercial glass ionomer cement, to evaluate *in vitro* its antibacterial activity against oral cavity strains. The NCu were synthesized by copper acetate reduction with L-ascorbic acid and characterized by FTIR, Raman, XPS, XRD and TEM. Then, commercial glass ionomer cement (GIC) was modified (MGIC) with various concentrations of NCu and physicochemically characterized. Cell viability was tested against human dental pulp fibroblasts (HDPFs) by Alamar-Blue assay and antibacterial test was performed against *S. mutans* and *S. sanguinis* by colony forming unit (CFU) growth method. Synthesized NCu rendered a mixture of both metallic copper and cuprous oxide (Cu$_2$O). HDPF viability reduces with exposure time to the extracts (68–72% viability) and MGIC with 2–4 wt% NCu showed antimicrobial activity against the two tested strains.

Keywords: Biomaterial, Dental cement, Metal nanoparticle, Fibroblast, Anaerobia bacteria

INTRODUCTION

The development of new dental cements with improved physical and esthetic properties is a matter of constant research. However, none of current commercially available cements can be considered permanent due to the appearance of secondary caries, which is the main cause of failure after treatment[1,2]. For some authors, this injury occurs adjacent to the filling material by the presence of biofilm at the interface of the restoration and dental tissue[3] and is characterized by the movement of fluid, bacteria and chemical substances between the restoration and the dental tissue (microleakage)[1]. Mo *et al*. describe the existing microflora in secondary caries lesions; they found *Prevotella, Veillonella, Lactobacillus, Streptococci mutans, Neisseriae* and *Actinomyces spp.,* as the predominant strains followed by *Peptostreptococcus, Fusobacterium* and *Porphyromonas gingivalis*[4]. However, their mere presence is not the only factor for caries formation, as it has been suggested that *S. sanguinis* is also an important strain[5]. In addition, several studies noted that after partially removing the decayed dental tissue, the materials tend to degrade and become rough when they are in contact with the accumulation of bacteria[6].

Thus, minimally invasive dentistry is called to be the treatment of choice when possible; consists in the preservation of the maximum percentage of healthy dental tissue and the restoration of the carious cavities under criteria that involve the partial removal of the affected tissue[7], in order to promote the remineralization of the remaining dental structure[8]. One of these treatments is the atraumatic restorative technique (ART), indications for which were described by Holmgren and Frencken in 1999[9]. Currently, the guidelines suggest the placement of high viscosity glass ionomer cement (GIC)[10] which exhibits similar coefficient of thermal expansion to dental tissue, long term release of fluoride and acceptable biocompatibility[11]. In spite of the incorporation of fluoride in GIC's, secondary caries is still an unsolved problem knowing that the amount of released fluoride is not enough to guarantee its anticariogenic activity[12]. Therefore, antibacterial additives have been proposed as alternative route to modify GIC formulations; including quaternary ammonium salts, natural products such as propolis[13,14], metals[15], antiseptics[16], *etc*.

Furthermore, the use of nanometric metallic particles such as Cu, have also been studied because they exhibit antibacterial activity[17], as the reduction in size increases the interaction area with bacteria[18]. Thus, copper oxide (Cu$_2$O) can been used in the biomedical field due to its proven antibacterial efficacy against Gram negative and positive bacteria like *Escherichia coli* and *Staphylococcus aureus,* respectively, and even the "super microbe" *S. aureus* resistant to methicillin (MRSA)[19], although its potential cytotoxicity is reported as the main disadvantage[17]. Therefore, the aim of this study is to synthesize copper nanoparticles (NCu) by a green method, characterize their physical-chemical properties, and to determine both the NCu antibacterial potential against *Streptoccocus mutans* and *Streptococcus sanguinis* and human dental pulp fibroblasts (HDPFs) viability once incorporated into the GIC.

MATERIALS AND METHODS

Synthesis of NCu

A solution of 0.1 M copper acetate (Sigma-Aldrich, Dublin, Ireland) was refluxed and stirred at 80°C, then a solution of L-ascorbic acid (Sigma-Aldrich) (2:1 M respect to copper acetate) was added. The mixture was kept in constant stirring for 30 min and then centrifuged at 8,000 rpm in 10 cycles of 20 min. The solid obtained was frozen at −80°C and then freeze-dried during 48 h.

Preparation of the modified glass ionomer cement (MGIC)

GIC (Fuji IX, GC, Tokyo, Japan) was prepared according to the manufacturer's specifications by hand mixing and filled with copper nanoparticles at 1, 2, 3 and 4 wt%. Discs of the GIC (without NCu) and MGIC were prepared in a silicone mold with 6.35 mm diameter and 2 mm thickness.

Physicochemical characterization of NCu, GIC and MGIC

Fourier-transform infrared (FTIR) spectra were obtained using a Nicolet 8700 (Thermo Scientific, Madison, WI, USA) spectrometer, in the spectral range between 4,000 and 400 cm^{-1} using KBr pellets. Raman spectra were collected between 3,200 cm^{-1} and 100 cm^{-1} using an inVia Renishaw Raman spectrometer (Renishaw, Gloucestershire, UK). A 633 nm argon laser at 5% power was used as the excitation radiation source. Elemental microanalysis was obtained by Energy-dispersive X-ray spectroscopy (EDX; INCA Energy 200, Oxford Instruments, Oxfordshire, UK) coupled to scanning electron microscope (JEOL JMS 6360LV, Japan Electron Optics Laboratory, Tokyo, Japan) at 20 kV. X-ray diffraction (XRD) patterns were obtained using a Bruker D8-Advance Bragg diffractometer (Bruker, Billerica, MA, USA) in the 2θ range from 5° to 60°, with an interval time lapse of 1 s and a step size of 0.02°. X-ray photoelectron spectroscopy (XPS) was conducted in a Thermo Scientific K-Alpha X-ray (Thermo Fisher Scientific, Orion, MA, USA) photoelectron spectrometer (with a monochromatic source of Al Kα with an energy of 1486.6 eV) on etched (Ar ions for 30 s) samples. Transmission electron microscopy (TEM) was conducted with a JEOL JEM-ARM200F (Japan Electron Optics Laboratory) with 200 keV at a 50 µm opening at 2×10^{-5} Pa vacuum. The samples were deposited in a platinum grid covered with Formvar film.

HDPF viability

HDPF were isolated from sound thirds molars, indicated to extraction due to orthodontic diagnosis. After tooth extraction, molars were placed in a 50 mL tube containing Dulbeccos' Modiffied Medium (DMEM; Thermo Scientific HyClone, Logan, UT, USA), antibiotics and antimycotic (100 IU/mL penicillin, 100 µg/mL streptomycin and 0.3 µg/mL fungizone). The pulp was obtained from a cut in the cervical third of the molar using a micromotor and a diamond disc and then the coronal part was removed, accessing to the root canal. The pulp tissue was extracted with endodontic files number 15 and 20. Then, the pulp was placed in a 5 mL tube with Trypsin-EDTA (0.25%) for 5 min incubation at 37°C. The tubes were centrifuged at 5,000 rpm, and then the supernatant was removed and the obtained pellet was resuspended in 1.5 mL of DMEM and supplemented with 10% fetal bovine serum (FBS; Gibco, Carlsbad, CA, USA), antibiotics and antimycotic (100 IU/mL penicillin, 100 µg/mL streptomycin and 0.3 µg/mL fungizone). The content was then placed in a 6-well plate with 2 mL of DMEM. The cultures were kept at 37°C in a 5% CO$_2$ atmosphere with a 100% humidity environment. Cells were grown for three weeks with culture medium changes every third day, until 80% of cell confluence was achieved and then transferred for the first passage to 75 cm^2 culture flask.

GIC discs were prepared 15 min prior UV sterilization (30 min) per side and placed in a tube containing 2.5 mL medium and incubate at 37°C for 72 h to obtain the extracts in triplicate.

Fibroblasts (1.5×10^3 cells/mL) were seeded in 100 µL of DMEM in 96-well plates and incubated at 37°C with 5% CO$_2$ for 24 h. After incubation, medium were removed and 100 µL of fresh DMEM and 100 µL of experimental extract was added[20]. Then, 20 µL of Alamar-Blue were deposited on each well and read at 570 nm using a Cytation 3 (Biotek). Cell viability at 0, 3, 6, 12, 24 and 48 h was recorded.

Antimicrobial assay

The assay was performed using discs (6.35 mm diameter and 1 mm thickness) of GIC and those with 1, 2, 3 and 4 wt% NCu (MGIC). Five groups with n=3 specimens per group were tested. Pure cultures of *S. mutans* (ATCC 25175) and *S. sanguinis* (ATCC 10556) were used for the antibacterial test. Lyophilized bacterial stocks (American Type Culture Collection, Rockville, MD, USA) were rehydrated in Mycoplasma broth base (BBL, Becton-Dickinson, Sparks, MD, USA). Both strains were grown on Mycoplasma agar base (BBL, Becton-Dickinson, Franklin Lakes, NJ, USA) supplemented with 5% defibrinated sheep blood, 5 mg/mL hemin, and 0.3 mg/mL menadione under anaerobic conditions (80% N$_2$, 10% CO$_2$, and 10% H$_2$). Bacterial growth from 5 to 7 day cultures of each strain was harvested and the optical density (OD) in each tube was adjusted to 1 at 600 nm in a spectrophotometer. Sterile experimental discs of either GIC or MGIC were placed individually in 48-well plates and a total of 1×10^6 cells/mL suspension of each reference strain was added, in a total volume of 1 mL. Plates were incubated for 48 h at 35°C under anaerobic conditions using enriched Mycoplasma broth-media (5 mg/mL hemin and 0.3 mg/mL menadione). After this period, the culture medium was removed and the experimental samples were transferred into a new plate with 1,000 µL of sterile medium and sonicated for 5 s three times. One hundred microliter of inoculated medium were placed in a Mycoplasma agar plate, spread over the surface and incubated for 48 h under anaerobic conditions. After incubation, the number of the CFUs was counted on all the plates, to determine the antibacterial

effect of the experimental samples.

Statistical analyses

The data were evaluated using Statistical Package Minitab software (Minitab, Coventry, UK). One-way analysis of variance and Tukey *post-hoc* tests at a significance level of $p=0.05$ were used to perform multiple comparison tests.

RESULTS

Physicochemical characterization of NCu

FTIR spectrum of copper nanoparticles is shown in Fig. 1a. A strong absorption at 628 cm^{-1} was observed, which can be related to copper oxide. In agreement with this, Raman spectrum (see Fig. 1b) of these particles showed strong absorptions at 144, 218, 519 and 606 cm^{-1}. By EDX it was found that NCu contained 67.1 at% Cu, 15.3 at% O and 17.6 at% C. The XPS analysis, as depicted in Fig. 1c, shows peaks at 952.18 and 932.48 eV with no satellites, which can be attributed to both, elemental copper or copper oxides. Characterization by TEM showed a mean particle size of 10.87 nm (Fig. 1d).

Physicochemical characterization of GIC and MGIC

Figure 2a shows the FTIR spectra of the NCu modified GIC (MGIC). These composites showed infrared absorptions at 1,720 cm^{-1}, attributed to C=O stretching of the carboxylic group and those at 1,635 cm^{-1} corresponding to C=C bonds. The peak shift registered at 1,166 cm^{-1} may be assigned to the C-O stretching of a carboxylic group corresponding to both, tartaric and poly(acrylic) acids. In addition to CH_2 vibrations, absorptions between 1,401 and 1,463 cm^{-1} are associated to Ca and Al salt formation. Moreover, absorptions between 400 to 800 cm^{-1} are assigned to Al_2O_3, metallic fluorides, Cu_2O, *etc.*

Raman spectra, as shown in Fig. 2b, showed two strong peaks; one at 2,932 cm^{-1}, attributed to CH_2, and other at 1,400 cm^{-1} due to the symmetrical stretching of CH_2 from the poly(acrylic) acid. The presence of copper oxide nanoparticles was evident as absorption at 526 and 620 cm^{-1}, which increased with copper concentration in the MGIC.

The diffractogram in Fig. 2c shows the XRD patterns of the MGIC. Non-modified GIC did not show reflection due to the amorphous composition of the material. However, as the amount of NCu increased, peaks at 43.3º (111) and 50.44º (200) appeared. Peaks corresponding to pristine NCu at 36.8° and 38.9° were not detected in MGIC.

Elemental content and distribution of Cu in GIC and MGIC are shown in Table 1, which goes from 0.76 to 1.53% for 1 and 4 wt% of NCu respectively. EDX mapping of elemental Cu showed a good distribution of
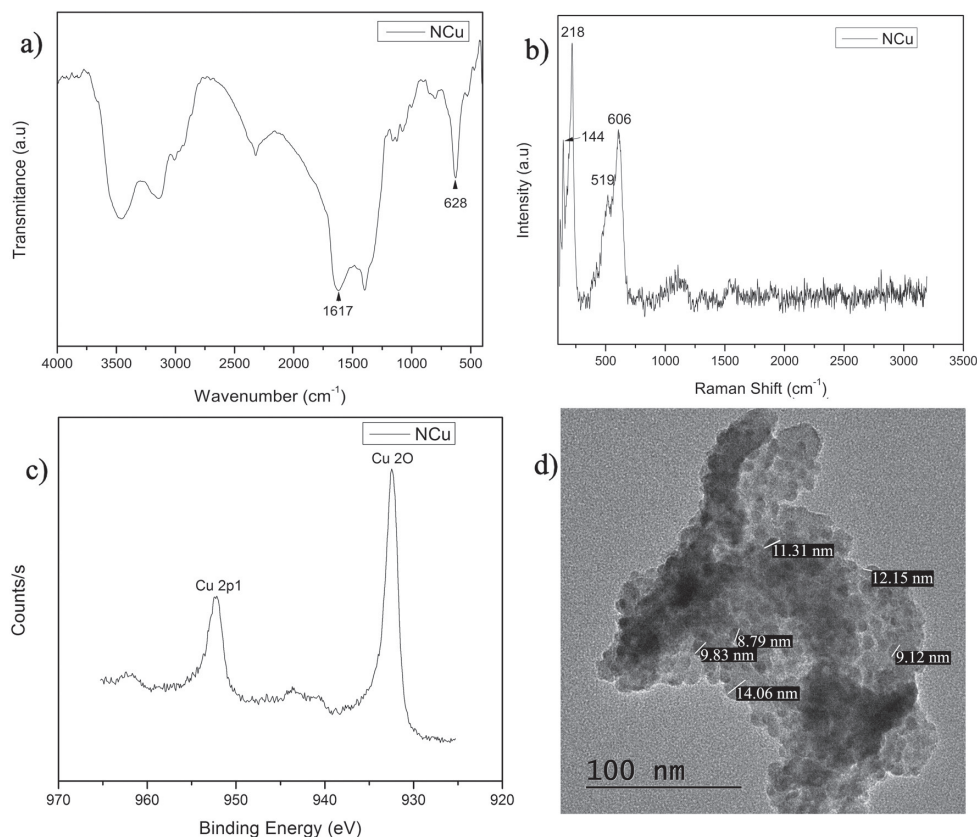

Fig. 1   Spectroscopy of copper nanoparticles (a) FTIR, (b) Raman, (c) XPS, (d) TEM image.
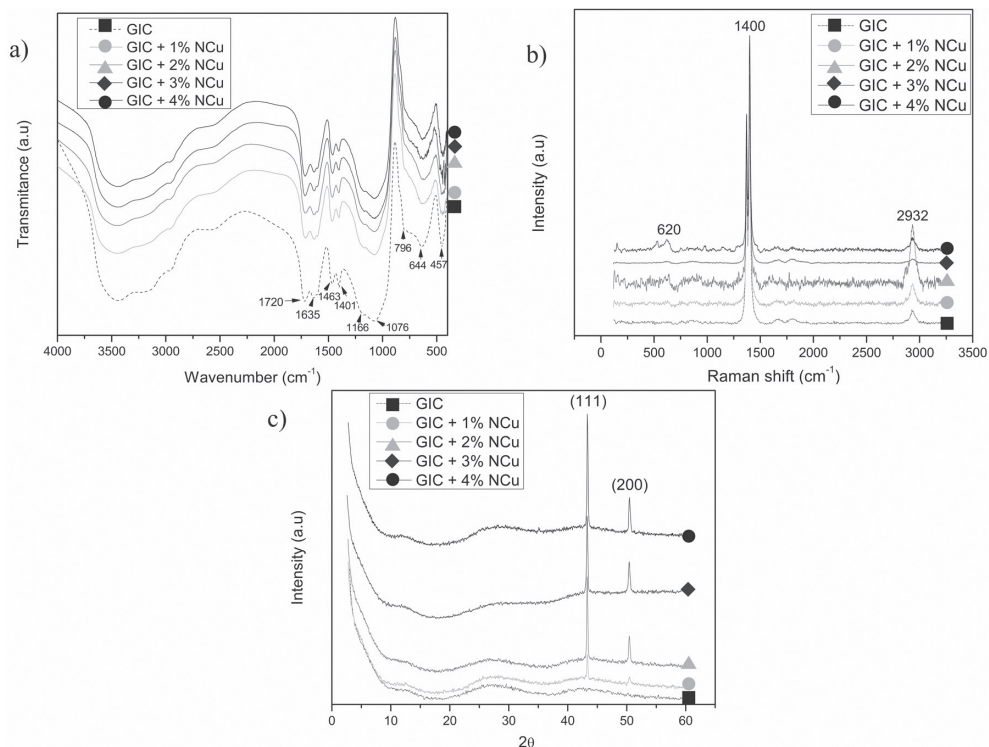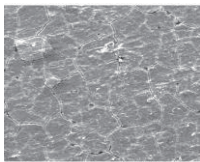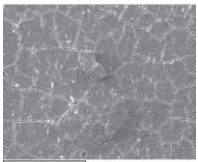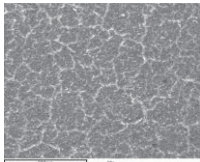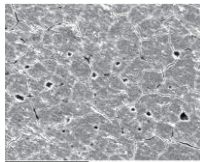
Fig. 2 Physicochemical characterization of GIC and MGIC with various NCu content.
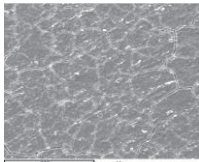(a) FTIR spectra (b) Raman spectra (c) XRD diffractogram.

Table 1 Elemental content (atomic %) of GIC and MGIC with NCu. Images above correspond to EDX mapping of Cu

	GIC	GIC + 1% NCu	GIC + 2% NCu	GIC + 3% NCu	GIC + 4% NCu
C	43.77	45.44	44.82	46.56	43.5
O	36.2	34.64	34.32	31.67	35.67
F	7.75	6.92	7.05	7.04	6.93
Na	1.6	1.52	1.59	1.68	1.56
Al	5.02	5.06	5.36	5.65	5.16
Si	3.86	3.92	4.1	4.44	3.9
P	0.09	0	0.09	0.17	0
Ca	0.14	0.09	0.22	0.03	0.18
Cu	0	0.76	0.85	0.98	1.53
Sr	1.57	1.65	1.6	1.78	1.57

NCu in MGIC matrix.

Viability of HDPF in contact with GIC and MGIC
HDPF viability tends to be reduced with time of exposure to the extracts and NCu content, as depicted in Fig. 3. Viability of cells exposed to GIC extracts was under 74% after 48 h, while cell viability when exposed to MGIC extracts ranged from 68 to 72%. The ANOVA for viability cell assay found that GIC and MGIC at 0, 3, 6, 12, 24 and 48 h, groups were no statistically different between times
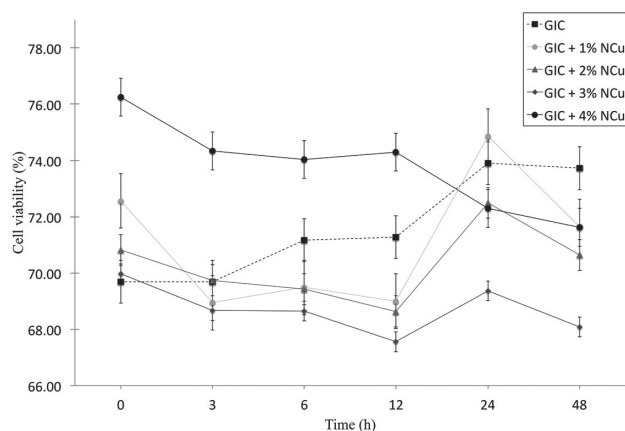

Fig. 3 Viability percentage of HDPF in presence of experimental extracts of GIC and MGIC at 0, 3, 6, 12, 24 and 48 h.
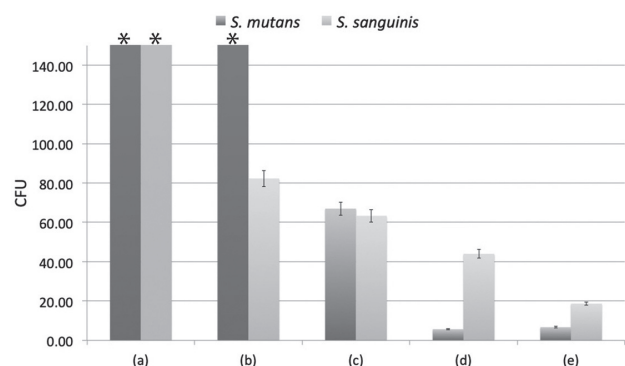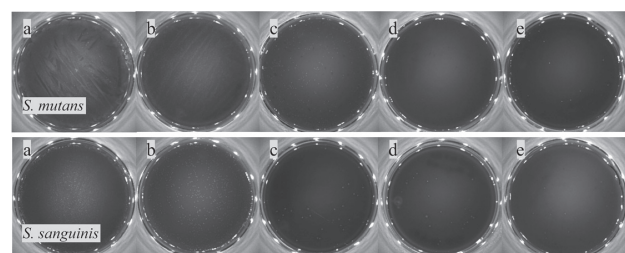

Fig. 4 CFU growth of both *S. mutans* and *S. sanguinis* strains at different NCu concentration in MGIC. (a) GIC, (b) GIC+1% NCu, (c) GIC+2% NCu, (d) GIC+3% NCu and (e) GIC+4% NCu. *CFU counting>1,000.

and the post-hoc test did not differ between groups.

Antibacterial activity
The antibacterial activity of the MGIC is shown in Fig. 4. CFU counting of both *S. mutans* and *S. sanguinis* strains showed a reduced growth up to 80% after getting in contact with GIC and MGIC with a copper content higher than 1 wt%. CFU values of *S. mutans* on pristine GIC and 1 wt% MGIC allowed a growth greater than 1,000 CFU but for 2–4 wt% MGIC, this decreased to less than 90 CFU, being statistically lower ($p=0.001$) than the first two groups. Furthermore, CFU values for *S. sanguinis* decrease to less than 80 CFU when strains are in contact with 2 wt% MGIC, which were also statistically different than those for 3–4 wt% MGIC ($p=0.05$). The ANOVA found that GIC and MGIC against *S. sanguinis* result statistically different ($p=0.042$) in *post-hoc* test between 1 wt% and those with 4 wt%.

DISCUSSION

The use of metals mixed with many biomaterials for improving antibacterial performance has been documented[21,22]. In the case of copper, its antibacterial activity is attributed to the disruption of cell membrane allowing the loss of organelles and nutrients[23]. In order to explain NCu effectiveness once incorporated to a GIC, they were fully characterized. Visual inspection of the as-prepared particles showed an orange color that with time (and oxygen exposure) darken. Although copper oxide is the main component, Fig. 1a also shows absorptions at 3,500 cm^{-1} (OH) and 1,617 cm^{-1} (C=C), which can be attributed to residuals from the synthesis. FTIR spectrum of pristine L-ascorbic acid showed bands at 3,303, 1,755 and 1,674 cm^{-1} and therefore copper nanoparticles still contained L-ascorbic acid and possibly water. Our FTIR results agree with those of Umer *et al.,* who reported stretching absorptions at 1,617 and 3,411 cm^{-1} for C=C and O-H stretching groups, respectively[24]. Similarly, Castaño *et al.,* who obtain NCu with starch as stabilizer, reported a strong absorption at 628 cm^{-1}, assigned to Cu-O vibrations, confirming the presence of Cu$_2$O[25].

In agreement with this, Raman spectrum of these particles (Fig. 1b) showed strong absorptions at 144, 218, 519 and 606 cm^{-1}, which according to Deng *et al.* those at 220 and 606 cm^{-1} corresponded to Cu$_2$O and CuO, respectively[26]. Further confirmation of the presence of Cu$_2$O and metallic Cu was obtained from the XPS peaks at 952.18 and 932.48 eV, with no satellites, in agreement with those reported by Jiang *et al.* and Biesinger *et al.*[27,28]. The mean particle size of our copper nanoparticles was 10.87 nm (Fig. 1d) but these, as prepared particles, tend to aggregate into very stable clusters. Our results differed from those reported by Kobayashi *et al.* as they obtained particles with an average size of 57.75 nm without using a stabilizing agent[29,30]. However, when oleic acid was used as surfactant with 1 and 2 M ascorbic acid as reducing agent, the mean particle sizes obtained were 15.3 and 67 nm, respectively[31].

FTIR (Fig. 2a) and Raman (Fig. 2b) spectroscopy also identified components present in typical glass ionomer cement. Hydroxyl absorptions, which are active in IR but not in Raman, were detected because of the presence of both poly-acrylic and tartaric acids. The intense bands at 1,720 and 1,635 cm^{-1} in the IR spectra, but of low intensity in the Raman spectra, suggested the presence of a poly(acrylic acid), tartaric acid and residual acrylic monomer. The small shoulder at 1,602 cm^{-1} can be due to a minor aromatic compound. Copper nanoparticles in the GIC were clearly identified by Raman spectroscopy as bands at either 526 or 620 cm^{-1} increased in intensity as the copper concentration in the MGIC increased. The amorphous nature of the alumino-silicate glass and poly(acrylic acid) was evident by the lack of apparent peaks in their XRD pattern, as shown in Fig. 2c. On the contrary, the crystalline nature of the copper nanoparticles produced diffraction peaks at 2θ=43.3º (111) and 50.44º (200) that can be attributed to Cu$_2$O and metallic copper, respectively[24,29,32,33]. By EDX, it was observed the presence of large quantities of Si (3.86 at%) and Al (5.02 at%), which corresponds to the alumino-silicate glass. In addition, Sr (1.57 at%) was detected as part of a contrast agent while F (7.75 at%) in sodium fluoride is added to these materials for preventing teeth decay[34-36]. The atomic percentage of Cu quantified by EDX did not correspond to the amount loaded, since the NCu was incorporated in weight percentage, according to GIC manufacturer's instructions. Furthermore, NCu elemental characterization showed the presence of carbon and oxygen lowering the expected amount in the MGIC.

For any antimicrobial dental material is desirable that mammalian cells are not killed while bacteria proliferation is prevented. As shown in Fig. 3, fibroblasts viability was higher than 70% confirming the non-cytotoxic effect of Fuji IX GIC 72 h extracts. Moreover, 4 wt% of NCu addition to MGIC produced extracts that did not significantly decrease HDPF viability. This is in agreement with Siqueira *et al.*, using immortalized odontoblasts MDPC-23 in contact with silver modified glass ionomer cement, as they reported cell viability between 60–95%[37]. However, this is in contrast to results reported by Kanjevac *et al.* as they correlated fluoride release with a cytotoxicity effect; *i.e.*, 82.7% cell death, against human dental pulp stem cells[20].

Regarding the antibacterial mechanism of copper nanoparticules we consider that the antibacterial effect was mainly attributed to surface contact. Previous reports consider 3 main types of antibacterial mechanisms of copper[17,38]. In the first mechanism, there is an accumulation and dissolution of nanoparticles. Therefore, the negative portion of cell membrane and positive metallic nanoparticle, contribute to the electron transfer and rupture of the bacteria membrane with subsequent release of lipopolysaccharides, membrane proteins and intracellular biomolecules; In the second mechanism, copper generate reactive oxygen species (ROSs) by Fenton-like reaction[38], producing membrane damage derived from the free radicals and then causing the liberation of internal content[17]; In the third mechanism, DNA damage is by the uptake of Cu ions or NCu. Based on this, it is possible that Cu$_2$O antibacterial properties are caused by ROS formation at the nanoparticle surface, especially at short times, but ion release at longer times is not discarded as 0.45 ppm of copper was detected by atomic absorption spectroscopy in 72 h extracts obtained from MGIC with 4% NCu. NCu incorporated into Fuji IX GIC were effective in reducing both *Streptoccocus mutans* and *Streptococcus sanguinis* growth between 2 and 4 wt% as reported in Fig. 4. These results also suggests that delayed colonization by *S. mutans* will not take a place, as *S. sanguinis* is also inhibited[39].

The NCu were mainly metallic copper and Cu$_2$O with an average size of 10.87 nm and it is not clear if residual ascorbic acid limits its effectiveness or if this is the optimum size. However, it is well known that ascorbic acid is a potent antioxidant, which may delay NCu oxidation and extend copper ions release. In spite of the small particle size achieved for the as prepared NCu, these particles were well dispersed in the MGIC suggesting a complete exposure to any bacteria, even if the GIC is fractured. However, Toodehzaeim *et al.* recommended the control of CuO nanoparticle sizes and their surface modification to avoid potential toxic effects[40]. Covarrubias *et al.* described the capacity of NCu to inhibit the growth or to reduce the number of viable *S. mutans* in a similar manner than the one found in our study. They concluded that hybrid copper-chitosan nanoparticles showed greater capacity for both, preventing biofilm formation and reducing bacteria viability than NCu[41]. In another study, Toodehzaeim *et al.* incorporated 1 wt% NCu to an orthodontic adhesive and determined an inhibition zone of 9.20 mm for *S. mutans*[40]. Similarly, NCu added to an etch and rise adhesive showed a significant antimicrobial behavior against *S. mutans*[42]. Fúcio *et al.* tested various GIC and resin MGIC against *S. mutans* and they observed a 7.8 mm inhibition zone for Fuji IX, by agar disc diffusion method, differing with our results, where no antimicrobial activity were found for the unmodified GIC[6]. In agreement with this, Zalewska reported inhibition zones of 11 and 12.3 mm for *S. mutans* and *S. sanguinis* respectively when commercial GIC were tested[43].

CONCLUSION

Nano particles synthesized by L-ascorbic acid reduction of copper acetate, render a mixture of both metallic copper and Cu$_2$O with an average size of 10.87 nm, determined by FTIR, Raman, EDX, XPS, XRD and TEM. In addition, NCu in the MGIC were observed in both surface and bulk as determined by EDX mapping. MGIC exhibited antibacterial behavior against oral anaerobic bacteria strains (*S. mutans* and *S. sanguinis*), when NCu were added between 2–4 wt%. At this concentration, HDPF retained viability above 68%.

REFERENCES

1) Shih WY. Microleakage in different primary tooth restorations. J Chinese Med Assoc 2016; 79: 228-234.
2) Nedeljkovic I, Teughels W, De Munck J, Van Meerbeek B, Van Landuyt KL. Is secondary caries with composites a material-based problem? Dent Mater 2015; 31: e247-277.
3) Jokstad A. Secondary caries and microleakage. Dent Mater 2016; 32: 11-25.
4) Mo S, Bao W, Lai G, Wang J, Li M. The microfloral analysis of secondary caries biofilm around Class I and Class II composite and amalgam fillings. BMC Infect Dis 2010; 10: 241.
5) Ge Y, Caufield PW, Fisch GS, Li Y. Streptococcus mutans and Streptococcus sanguinis colonization correlated with caries experience in children. Caries Res 2008; 42: 444-448.
6) Fúcio SBP, de Paula AB, Sardi JCO, Duque C, Correr-Sobrinho L, Puppin-Rontani RM. Streptococcus Mutans biofilm influences on the antimicrobial properties of glass ionomer cements. Braz Dent J 2016; 27: 681-687.
7) Innes NP, Manton DJ. Minimum intervention children's dentistry —The starting point for a lifetime of oral health. Br Dent J 2017; 223: 205-213.
8) Ngo HC, Mount G, Mc Intyre J, Tuisuva J, Von Doussa RJ. Chemical exchange between glass-ionomer restorations and residual carious dentine in permanent molars: an in vivo study. J Dent 2006; 34: 608-613.
9) Holmgren CJ, Frencken JE. Painting the future for ART. Community Dent Oral Epidemiol 1999; 27: 449-453.
10) Hilgert LA, De Amorim RG, Leal SC, Mulder J, Creugers NHJ, Frencken JE. Is high-viscosity glass-ionomer-cement a successor to amalgam for treating primary molars? Dent Mater 2014; 30: 1172-1178.
11) Calvo AFB, Kicuti A, Tedesco TK, Braga MM, Raggio DP. Evaluation of the relationship between the cost and properties of glass ionomer cements indicated for atraumatic restorative treatment. Braz Oral Res 2016; 30: 3-9.
12) Farrugia C, Camilleri J. Antimicrobial properties of conventional restorative filling materials and advances in antimicrobial properties of composite resins and glass ionomer cements —A literature review. Dent Mater 2015; 31: e89-99.
13) Hatunoglu E, Oztürk F, Bilenler T, Aksakalli S, Simsek N. Antibacterial and mechanical properties of propolis added to glass ionomer cement. Angle Orthod 2014; 84: 368-373.
14) Altunsoy M, Uslu ME, Silici S, Altunsoy M. In vitro evaluation of microleakage and microhardness of ethanolic extracts of propolis in different proportions added to glass ionomer cement. J Clin Pediatr Dent 2016; 40: 136-140.
15) Elsaka SE, Hamouda IM, Swain MV. Titanium dioxide nanoparticles addition to a conventional glass-ionomer restorative: influence on physical and antibacterial properties. J Dent 2011; 39: 589-598.
16) Du X, Huang X, Huang C, Frencken JE, Yang T. Inhibition of early biofilm formation by glass-ionomer incorporated with chlorhexidine in vivo: a pilot study. Aust Dent J 2012; 57: 58-64.
17) Vimbela GV, Ngo SM, Fraze C, Yang L, Stout DA. Antibacterial properties and toxicity from metallic nanomaterials. Int J Nanomedicine 2017; 12: 3941-3965.
18) Kruk T, Szczepanowicz K, Stefańska J, Socha RP, Warszyński P. Synthesis and antimicrobial activity of monodisperse copper nanoparticles. Colloids Surf B Biointerfaces 2015; 128: 17-22.
19) Hans M, Erbe A, Mathews S, Chen Y, Solioz M, Mücklich F. Role of copper oxides in contact killing of bacteria. Langmuir 2013; 29: 16160-16166.
20) Kanjevac T, Milovanovic M, Volarevic V, Lukic ML, Arsenijevic N, Markovic D, *et al.* Cytotoxic effects of glass ionomer cements on human dental pulp stem cells correlate with fluoride release. Med Chem 2012; 8: 40-45.
21) Popescu RA, Magyari K, Vulpoi A, Trandafir DL, Licarete E, Todea M, *et al.* Bioactive and biocompatible copper containing glass-ceramics with remarkable antibacterial properties and high cell viability designed for future in vivo trials. Biomater Sci 2016; 4: 1252-1265.
22) Abd-El-Aziz AS, Agatemor C, Etkin N. Antimicrobial resistance challenged with metal-based antimicrobial macromolecules. Biomaterials 2017; 118: 27-50.
23) Sajid M, Ilyas M, Basheer C, Tariq M, Daud M, Baig N, *et al.* Impact of nanoparticles on human and environment: review of toxicity factors, exposures, control strategies, and future prospects. Environ Sci Pollut Res 2015; 22: 4122-4143.
24) Umer A, Naveed S, Ramzan N. A green method for the synthesis of Copper Nanoparticles using L-ascorbic acid. Rev Mater 2014; 19: 197-203.
25) Castaño VM, Aguilar-Méndez MA, Ortega-Arroyo L, López-Andrade X, Narayanan J, Ceja-Romero LR, *et al.* Green chemistry synthesis of nano-cuprous oxide. IET Nanobiotechnol 2016; 10: 39-44.
26) Deng Y, Handoko AD, Du Y, Xi S, Yeo BS. *In situ* raman spectroscopy of copper and copper oxide surfaces during electrochemical oxygen evolution reaction: Identification of Cu^{III} oxides as catalytically active species. ACS Catal 2016; 6: 2473-2481.
27) Jiang P, Prendergast D, Borondics F, Porsgaard S, Giovanetti L, Pach E, *et al.* Experimental and theoretical investigation of the electronic structure of Cu_2O and CuO thin films on Cu(110) using x-ray photoelectron and absorption spectroscopy. J Chem Phys 2013; 138: 024704.
28) Biesinger MC. Advanced analysis of copper X-ray photoelectron spectra. Surf Interface Anal 2017; 49: 1325-1334.
29) Kobayashi Y, Shirochi T, Yasuda Y, Morita T. Preparation of metallic copper nanoparticles in aqueous solution and their bonding properties. Solid State Sci 2011; 13: 553-558.
30) Kobayashi Y, Shirochi T, Yasuda Y, Morita T. Metal–metal bonding process using metallic copper nanoparticles prepared in aqueous solution. Int J Adhes Adhes 2012; 33: 50-55.
31) Yu T, Koh T, Lim B. Synthesis of copper nanoparticles with controlled sizes by reverse micelle method. J Nanosci Nanotechnol 2013; 13: 3250-3253.
32) Khan A, Rashid A, Younas R, Chong R. A chemical reduction approach to the synthesis of copper nanoparticles. Int Nano Lett 2016; 6: 21-26.
33) Theivasanthi T, Alagar M. X-ray diffraction studies of copper nanopowder. Arch Phys Res 2010; 1: 112-117.
34) Zanata RL, Magalhães AC, Lauris JRP, Atta MT, Wang L, Navarro MFDL. Microhardness and chemical analysis of high-viscous glass-ionomer cement after 10 years of clinical service as ART restorations. J Dent 2011; 39: 834-840.
35) Ahmad Shiekh R, Ab Rahman I, Malik Masudi S, Luddin N. Modification of glass ionomer cement by incorporating hydroxyapatite-silica nano-powder composite: Sol–gel synthesis and characterization. Ceram Int 2014; 40: 3165-3170.

36) Zoergiebel J, Ilie N. An in vitro study on the maturation of conventional glass ionomer cements and their interface to dentin. Acta Biomater 2013; 9: 9529-9537.

37) Siqueira PC, Magalhaes APR, Pires WC, Pereira FC, Silveira-Lacerda EP, Carriao MS, *et al.* Cytotoxicity of glass ionomer cements containing silver nanoparticles. J Clin Exp Dent 2015; 7: e622-627.

38) Nguyen KVT, Ameer FS, Anker JN, Brumaghim JL, Minh HC. Reactive oxygen species generation by copper(II) oxide nanoparticles determined by DNA damage assays and EPR spectroscopy. Nanotoxicology 2017; 11: 278-288.

39) Loesche WJ. Role of Streptococcus mutans in human dental decay. Microbiol Rev 1986; 50: 353-380.

40) Toodehzaeim MH, Zandi H, Meshkani H, Firouzabadi AH. The effect of CuO nanoparticles on antimicrobial effects and shear bond strength of orthodontic adhesives. J Dent 2018; 19: 1-5.

41) Covarrubias C, Trepiana D, Corral C. Synthesis of hybrid copper-chitosan nanoparticles with antibacterial activity against cariogenic Streptococcus mutans. Dent Mater J 2018; 37: 379-384.

42) Gutiérrez MF, Malaquias P, Hass V, Matos TP, Lourenço L, Reis A, *et al.* The role of copper nanoparticles in an etch-and-rinse adhesive on antimicrobial activity, mechanical properties and the durability of resin-dentine interfaces. J Dent 2017; 61: 12-20.

43) Zalewska A. Antibacterial activity of selected glass ionomer cements. Postep Hig Med Dosw 2014; 68: 23-28.